Quantum-classical Liouville approach to molecular dynamics: Surface hopping Gaussian phase-space packets

Illia Horenko, Christian Salzmann, Burkhard Schmidt,[a] and Christof Schütte
Freie Universität Berlin, Institut für Mathematik II, Arnimallee 2–6, D-14195 Berlin, Germany

In mixed quantum-classical molecular dynamics few but important degrees of freedom of a molecular system are modeled quantum mechanically while the remaining degrees of freedom are treated within the classical approximation. Such models can be systematically derived as a first-order approximation to the partial Wigner transform of the quantum Liouville-von Neumann equation. The resulting adiabatic quantum-classical Liouville equation (QCLE) can be decomposed into three individual propagators by means of a Trotter splitting: (1) phase oscillations of the coherences resulting from the time evolution of the quantum-mechanical subsystem, (2) exchange of densities and coherences reflecting non adiabatic effects in quantum-classical dynamics, and (3) classical Liouvillian transport of densities and coherences along adiabatic potential energy surfaces or arithmetic means thereof. A novel stochastic implementation of the QCLE is proposed in the present work. In order to substantially improve the traditional algorithm based on surface hopping trajectories [J. C. Tully, J. Chem. Phys. **93**, 1061 (1990)], we model the evolution of densities and coherences by a set of surface hopping Gaussian phase-space packets (GPPs) with variable width and with adjustable real or complex amplitudes, respectively. The dense sampling of phase space offers two main advantages over other numerical schemes to solve the QCLE. First, it allows us to perform a quantum-classical simulation employing a constant number of particles; i.e., the generation of new trajectories at each surface hop is avoided. Second, the effect of nonlocal operators on the exchange of densities and coherences can be treated beyond the momentum jump approximation. For the example of a single avoided crossing we demonstrate that convergence towards fully quantum-mechanical dynamics is much faster for surface hopping GPPs than for trajectory-based methods. For dual avoided crossings the Gaussian-based dynamics correctly reproduces the quantum-mechanical result even when trajectory-based methods not accounting for the transport of coherences fail qualitatively. © *2002 American Institute of Physics.*
[DOI: 10.1063/1.1522712]

I. INTRODUCTION

One of the ultimate challenges in the field of modeling molecular dynamics is to explore the role of quantum effects. While fully quantum-mechanical investigations are presently, and most probably also in the near future, limited to the study of relatively small molecules,[1] the vast majority of studies of larger systems is still restricted to the regime of the classical approximation.[2] However, driven by recent experimental progress mainly in the field of ultrafast spectroscopy, there is a strong impact to include at least the most important quantum effects in studies of larger and, eventually, biologically relevant molecules.[3] The development of corresponding theoretical models still poses a great challenge.[4] Most of the present approaches consider the dynamics of a small subsystem (''system'') interacting with the remaining degrees of freedom (''bath'') using reduced density matrix techniques[5] to describe relaxation and dephasing. In most cases, however, these models rely on strongly simplified models for the coupling between the dynamics of system and bath and do not provide a fully microscopic model.

Mixed quantum-classical schemes offer a complementary approach. The underlying idea is to attribute quantum effects to a subsystem of the molecule under consideration, whereas it is sufficient to treat the remaining degrees of freedom by means of standard classical molecular dynamics. Usually the separation of the subsystems is motivated by the disparate mass scales, e.g., the electronic dynamics in studies of vibronic effects or the proton dynamics in investigations of hydrogen transfer systems. The main advantage of such a method is that it treats at least the most important degrees of freedom quantum mechanically, even for very large biomolecular systems.[6,7] In particular, nonadiabatic effects which are known to be of paramount importance in many photophysical, photochemical, and photobiological applications can be accounted for.[8,9] At the same time, the overall numerical effort does not considerably exceed that of a purely classical trajectory simulation.

The earliest variants of such hybrid schemes were based on the assumption of separability of the wave functions for the two subsystems interacting with each other through mean-field potentials and employ a classical approximation for the heavy-particle subsystem.[10–12] More recently the asymptotic properties of such models have been studied with more mathematical rigor.[13–15] Applications range from the

---

[a]Author to whom correspondence should be addressed. Electronic mail: burkhard@math.fu-berlin.de

study of reaction dynamics[16] and vibrational relaxation[17] up to proton-transfer processes in enzymes.[18–20]

The empirically based surface hopping scheme represents a first attempt to overcome the limitation of separability.[21–23] Owing to the intuitive concept of surface hopping as well as the favorable scaling properties of the numerical effort of this trajectory-based implementation, modified versions of the original algorithm are still commonly used in many studies of nonadiabatic molecular dynamics[24–32] where the recently devised continuous surface switching technique can be regarded as a hybrid version of mean-field and surface hopping methods.[33–35]

During the last few years mixed quantum-classical approaches to molecular dynamics were given a more rigorous foundation through the advent of the quantum-classical Liouville equation (QCLE).[36–40] Based on the elegant formulation of the classical limit of quantum mechanics in phase space by means of the Wigner transform,[41–46] the QCLE can be obtained as a partial Wigner transform of the original quantum Liouville-von Neumann equation.[47–50] Note that recently this approach has been extended towards statistical mechanics of mixed quantum-classical systems, including coupling to a dissipative environment.[51,52]

Related recent work is devoted to the construction of practical algorithms to solve the QCLE numerically using "multithreading" stochastic particle schemes.[53–55] The idea behind these methods is to propagate interacting δ-like particles in phase space to model the evolution of densities and coherences separately. While these approaches open the way towards higher dimensionality by providing an in principle correct stochastic realization of the QCLE, there is a severe limitation: Typically, at each nonadiabatic event, a copy of a particle has to be created, thus leading to a steeply increasing number of threads with time. One way to improve the sampling of phase-space distribution functions is to replace the δ-like trajectories by finite-width basis functions, exploring more or less large volumes of phase space at once.[56,57] A first realization of this technique in the field of nonadiabatic quantum dynamics is "multiple spawning" using a basis of frozen Gaussian packets[58] which is allowed to dynamically expand and contract.[59,60] Applications of the full multiple spawning method to biomolecular processes have been reported in Ref. 61.

In the present paper we seek for a combination of the respective advantages of the approaches described above to construct a novel, stochastic algorithm to solve the QCLE. On the one hand, the trajectory-based surface hopping approach keeps the number of particles constant, thus limiting the numerical effort. On the other hand, Gaussian packets offer a much better sampling of phase space and, furthermore, allow the evaluation of nonlocal operators. Hence, an efficient simulation technique will consist of propagating sets of Gaussian phase space packets (GPPs) to model the time evolution of densities and coherences where the amplitudes of the latter ones may be complex to incorporate quantum-mechanical phase effects. A stochastic criterion will govern the hopping of GPPs between different states of the quantum subsystem. Moreover, an adjustment of the amplitudes of the GPPs can be used to avoid spawning.[39] Thus, the propaga-

tion of surface hopping GPPs is expected to inherit the favorable scaling properties of trajectory-based implementations of the QCLE, while avoiding the increase of the number of particles with simulation time. Hence, it provides a promising tool for the description of medium to large molecules.

The remainder of this paper is organized as follows: Section II presents a fully quantum-mechanical model of molecular dynamics based on a diabatic or adiabatic representation of the density and Hamiltonian operator. Subsequently, a quantum-classical description is derived in Sec. III by means of partial Wigner transforms. Section IV presents numerical schemes to solve the QCLE and their implementation in terms of surface hopping techniques. Numerical simulations in Sec. V illustrate the use of these methods.

II. FULL QUANTUM DYNAMICS

A. Quantum Liouville equation

Let us consider a physical or chemical multicomponent system composed of a heavy particle of mass M and a light particle of mass m which are described by two sets of position and momentum operators $\hat{R}, \hat{P}$ and $\hat{r}, \hat{p}$, respectively. Generalization to the case of several heavy and/or light-particles is straightforward by expressing positions and momenta in terms of vectors of length d or D, respectively. The dynamics of the system can be characterized by the following quantum-mechanical Hamiltonian operator:

$$\hat{H}(\hat{r},\hat{p},\hat{R},\hat{P}) = \hat{V}(\hat{r},\hat{p},\hat{R}) + \frac{1}{2M}\hat{P}^2, \qquad (2.1)$$

where the kinetic energy of the heavy particle is separated from the Hamiltonian of the light-particles which may be considered as potential energy acting on the heavy particle,

$$\hat{V}(\hat{r},\hat{p},\hat{R}) = \hat{U}(\hat{r},\hat{R}) + \frac{1}{2m}\hat{p}^2, \qquad (2.2)$$

with the potential energy operator $\hat{U}$ depending on the positions of both components.

The dynamics of the system is governed by the quantum-mechanical Liouville-von Neumann equation

$$\partial_t \hat{\rho}(t) = -\frac{i}{\hbar}[\hat{H},\hat{\rho}(t)]_- \equiv -\frac{i}{\hbar}\hat{\mathcal{L}}\hat{\rho}(t), \qquad (2.3)$$

where the commutator $[\cdot,\cdot]_-$ of the density operator $\hat{\rho}$ with the Hamiltonian $\hat{H}$ of the system under consideration can also be regarded as a Liouvillian (super)operator $\hat{\mathcal{L}}$ acting on $\hat{\rho}$. Note that in the present paper we shall restrict ourselves to the case of a pure quantum state,

$$\hat{\rho}(t) = |\psi(t)\rangle\langle\psi(t)|, \qquad (2.4)$$

where the quantum Liouville equation is equivalent to the time-dependent Schrödinger equation. However, a generalization to the case of mixed states, e.g., for a thermal ensemble of quantum states, is possible.[51]

As a first step we introduce a position-space representation for the heavy-particle degrees of freedom, enabling us to write states and densities as

$$\psi(R,t)=\langle R|\psi(t)\rangle \quad \text{and} \quad \rho(R,R',t)=\langle R|\hat{\rho}(t)|R'\rangle, \tag{2.5}$$

where Dirac's bra-ket notation refers to a scalar product in the Hilbert space spanned by R. The corresponding Hamiltonian operator of Eq. (2.1) becomes

$$\hat{H}(R,R')=\left(\hat{U}(\hat{r},R)+\frac{1}{2m}\hat{p}^2-\frac{\hbar^2}{2M}\Delta_R\right)\delta(R-R'). \tag{2.6}$$

The above expressions for $\hat{\rho}(R,R')$ and $\hat{H}(R,R')$ have to be understood as a family of quantum-mechanical operators acting in the reduced Hilbert space spanned by the light-particle coordinate r and which are parametrically dependent on the heavy-particle coordinates R,R'. Note that later in the course of this work a partial Wigner transform in the heavy degrees of freedom shall be used while the quantum-mechanical nature of light-particles as reflected by the operators $\hat{r},\hat{p}$ shall be retained.

Following our earlier work, we now introduce an appropriate scaling of time and energy,[13]

$$\tilde{t}=\frac{\hbar}{\sqrt{mM}}t \quad \text{and} \quad \tilde{U}=\frac{m}{\hbar^2}U, \tag{2.7}$$

which leads to the scaled quantum Liouville equation

$$\partial_{\tilde{t}}\hat{\rho}(\tilde{t})=-\frac{i}{\epsilon}[\hat{\tilde{H}},\hat{\rho}(\tilde{t})]_-, \tag{2.8}$$

where the dimensionless number

$$\epsilon=\sqrt{\frac{m}{M}} \tag{2.9}$$

serves as a smallness parameter. In particular, the limit $\epsilon \to 0$ leads to the adiabatic limit of quantum dynamics.[13,50] The scaled Hamiltonian occurring in Eq. (2.8) is given by

$$\hat{\tilde{H}}(R,R')=\frac{m}{\hbar^2}\hat{H}(R,R')=\left(\hat{\tilde{V}}(R)-\frac{\epsilon^2}{2}\Delta_R\right)\delta(R-R'), \tag{2.10}$$

with the scaled potential

$$\hat{\tilde{V}}(R)=\frac{m}{\hbar^2}\hat{V}(R)=\hat{\tilde{U}}(R)+\frac{1}{2\hbar^2}\hat{p}^2. \tag{2.11}$$

After having given a representation of the Hamiltonian and density operators in the heavy-particle coordinates R, the following two subsections deal with diabatic and adiabatic representations of the operators $\hat{r},\hat{p}$ in the light-particle degrees of freedom. Furthermore, note that we will suppress the tildes on the scaled quantities throughout the remainder of this article for notational simplicity.

B. Hamiltonian operator

In the following we will assume an orthonormal, complete basis set $\{|\phi^{\text{dia}}\rangle\}$ to represent light-particle wave functions and operators in r,

$$\langle \phi_i^{\text{dia}}|\phi_j^{\text{dia}}\rangle=\delta_{ij}, \tag{2.12}$$

where Dirac's bra-ket notation is used here and throughout the remainder of this paper for the scalar product in r only. Using this *diabatic basis* set, the light-particle Hamiltonian [second and third terms on the right-hand side (RHS) of Eq. (2.10)] can be represented by a matrix with entries

$$V_{ij}(R)=\langle \phi_i^{\text{dia}}|\hat{V}(R)|\phi_j^{\text{dia}}\rangle. \tag{2.13}$$

Hence, the diabatic matrix representation of the total Hamiltonian (2.10) can be written as

$$H^{\text{dia}}(R,R')=\left(V(R)-\frac{\epsilon^2}{2}\Delta_R\right)\delta(R-R'). \tag{2.14}$$

It is noted that each of the entries of the matrices $V(R)$ and $H^{\text{dia}}(R)$ corresponds to an operator acting on the heavy-particle degrees of freedom. Hence, in the diabatic representation of quantum dynamics, the heavy-particles are represented by densities (or wave functions) moving along the diabatic potential energy surfaces $V_{ii}(R)$ coupled through the off-diagonal elements $V_{ij}(R)$.

The *adiabatic basis* is defined by a unitary transformation of the diabatic basis such that the representation of the light-particle Hamiltonian is diagonal with eigenvalues

$$E_i(R)\delta_{ij}=\langle \phi_i^{\text{adi}}(R)|\hat{V}(R)|\phi_j^{\text{adi}}(R)\rangle, \tag{2.15}$$

which define our adiabatic (Born-Oppenheimer) potential energy surfaces. The new basis parametrically depends on the heavy-particle positions R because the diabatic potential energy matrix (2.13) has to be diagonalized for every value of R. The corresponding matrix representation of the total Hamiltonian (2.10) is given by

$$H^{\text{adi}}(R,R')=\left(E(R)-\frac{\epsilon^2}{2}[\Delta_R+2C(R)\cdot\nabla_R+T(R)]\right)$$
$$\times \delta(R-R'), \tag{2.16}$$

where E is a diagonal matrix with entries $E_i(R)$ and the last two terms are due to the action of the kinetic operator Δ_R on the R-dependent adiabatic basis functions $|\phi^{\text{adi}}(R)\rangle$ which is the origin of nonadiabatic effects in this representation of quantum dynamics. In particular, the matrix elements of the first- and second-order nonadiabaticity operators are given by

$$C_{ij}^k(R)=\langle \phi_i^{\text{adi}}(R)|\nabla_{R_k}|\phi_j^{\text{adi}}(R)\rangle, \tag{2.17}$$

$$T_{ij}(R)=\langle \phi_i^{\text{adi}}(R)|\Delta_R|\phi_j^{\text{adi}}(R)\rangle, \tag{2.18}$$

where the dot product in third term on the RHS of Eq. (2.16) has to be understood as $C_{ij}(R)\cdot\nabla_R=\Sigma_{k=1}^D C_{ij}^k(R)\nabla_{R_k}$. The first-order coupling operator is anti-Hermitian with respect to interchange of the indices i,j,

$$C_{ij}^k=-(C_{ji}^k)^*, \tag{2.19}$$

while there exists no such relation for the matrix T. To summarize the adiabatic picture of quantum dynamics, the heavy-particles are represented by densities (or wave packets) moving along the adiabatic potential-energy surfaces $E_i(R)$ while the nonadiabaticity operators $C(R),T(R)$ induce nonadiabatic couplings.

C. Density operator

In analogy to what was shown in the previous section we will derive representations of the density operator using either one of the two basis sets for the state vectors of the light particle. We begin by expanding the total wave function of the system using the *diabatic representation* (2.12),

$$\chi_i^{\text{dia}}(R,t) = \langle \phi_i^{\text{dia}} | \psi(R,t) \rangle, \tag{2.20}$$

where the expansion coefficients $\chi_i^{\text{dia}}(R,t)$ are readily identified as time-dependent wave functions of the heavy-particles. The corresponding density matrix in the diabatic basis is given by

$$\rho_{ij}^{\text{dia}}(R,R')(t) = \langle \phi_i^{\text{dia}} | \hat{\rho}(R,R',t) | \phi_j^{\text{dia}} \rangle \equiv X_{ij}^{\text{dia}}(R,R',t), \tag{2.21}$$

in which every matrix element X_{ij}^{dia} stands for a (diabatic) position-space density matrix of the heavy-particles in R,R':

$$X_{ij}^{\text{dia}}(R,R',t) = \chi_i^{\text{dia}}(R,t)(\chi_j^{\text{dia}}(R',t))^*. \tag{2.22}$$

Alternatively, the total wave function can be written in *adiabatic representation*

$$\chi_i^{\text{adi}}(R,t) = \langle \phi_i^{\text{adi}}(R) | \psi(R,t) \rangle. \tag{2.23}$$

Accordingly, the density matrix can be expanded in the adiabatic basis set obtained for some value of R,

$$
\begin{aligned}
\rho_{ij}^{\text{adi}(R)}(R',R'',t) &= \langle \phi_i^{\text{adi}}(R) | \hat{\rho}(R',R'',t) | \phi_j^{\text{adi}}(R) \rangle \\
&= \sum_{mn} \Phi_{im}(R,R') X_{mn}^{\text{adi}}(R',R'',t) \\
&\quad \times \Phi_{nj}(R'',R),
\end{aligned} \tag{2.24}
$$

where X^{adi} is defined in analogy to X^{dia} in Eq. (2.22) but for the adiabatic heavy-particle densities. The scalar products of adiabatic basis functions for different positions R can be expanded in a Taylor series using Eqs. (2.17) and (2.19),

$$
\begin{aligned}
\Phi_{ij}(R,R') &= \langle \phi_i^{\text{adi}}(R) | \phi_j^{\text{adi}}(R') \rangle = \delta_{ij} + (R'-R) \cdot C_{ij}(R) \\
&\quad + \mathcal{O}((R'-R)^2),
\end{aligned} \tag{2.25}
$$

where the dot product has to be understood in a similar way as in Eq. (2.16). Finally, the expression for the adiabatic representation of the density is obtained as

$$
\begin{aligned}
\rho_{ij}^{\text{adi}(R)}(R',R'',t) &= X_{ij}^{\text{adi}}(R',R'',t) + (R'-R) \\
&\quad \cdot (C(R) X^{\text{adi}}(R',R'',t))_{ij} - (R''-R) \\
&\quad \cdot (X^{\text{adi}}(R',R'',t) C(R))_{ij} + \mathcal{O}(\delta R^2),
\end{aligned} \tag{2.26}
$$

where the notation δR indicates the order of magnitude of $R'-R$ or $R''-R$. In contrast to the diabatic representation, the elements of the adiabatic density matrix ρ^{adi} do not simply equal the corresponding heavy-particle density X^{adi} but contain additional terms originating from the R dependence of the adiabatic basis functions. In order to be consistent with the error estimates in the forthcoming sections we have given here only the expression up to first order in δR. However, it is straightforward to calculate higher terms. Furthermore, it

is noted that we have $\rho_{ij}^{\text{adi}} = X_{ij}^{\text{adi}}$ for vanishing nonadiabaticity, e.g., for the regions far off avoided crossings or intersections.

III. PARTIAL WIGNER TRANSFORMS

A. Definition

The Wigner transform is a well-established tool to represent quantum dynamics in phase space.[41–44] In particular, it can be shown that the equations of motion for Wigner distribution functions have a well-defined classical limit for $\hbar \to 0$. In order to derive a quantum-classical formulation for the dynamics of a system comprising of light and heavy-particles, we shall employ a partial Wigner transform with respect to the coordinates of the latter and consider the limit $\epsilon \to 0$. As will become more transparent in the following, such a representation of dynamics allows for a description of the degrees of freedom of the heavy-particles in the classical limit while still incorporating quantum effects connected with the light-particle dynamics.[47,50] Thus the partial Wigner transform provides a suitable tool for a quantum-classical description of dynamics. Using the scaling introduced in Eq. (2.7), the partial Wigner transform $A_W(R,P,t)$ of the (diabatic or adiabatic) matrix representation $A(R,R',t)$ of a quantum-mechanical operator $\hat{A}(\hat{r},\hat{p},\hat{R},\hat{P},t)$ can be written as

$$A_W(R,P,t) = \int_{\mathbf{R}^D} A\left(R - \frac{\epsilon}{2}\Xi, R + \frac{\epsilon}{2}\Xi, t\right) e^{iP \cdot \Xi} d\Xi, \tag{3.1}$$

where an additional factor $(2\pi)^{-D}$ has to be used to obtain the correct normalization for the Wigner distribution function ρ_W as a partial Wigner transform of the density matrix ρ. Note again that $A_W(R,P,t)$ stands for a matrix of functions in classical phase space with each of the matrix elements corresponding to a pair of (diabatic or adiabatic) states of the system.

In the next two sections, the effect of the partial Wigner transforms on the Hamiltonian and on the density operator is explained separately before finally the quantum-classical equations of motion are derived.

B. Hamiltonian operator

In this section we want to apply the technique of partial Wigner transforms to the total Hamiltonian (2.10) of a system of light and heavy-particles. The transform of the diabatic representation given in Eq. (2.14) is straightforward

$$H_W^{\text{dia}}(R,P) = V(R) + \tfrac{1}{2} P^2. \tag{3.2}$$

When Wigner transforming the adiabatic representation (2.16) of the total Hamiltonian of the system, we make use of the relation for the Wigner transform of a product of operators,[41–45]

$$(AB)_W = A_W e^{(\epsilon/2i)\Lambda} B_W = A_W B_W + \frac{\epsilon}{2i} A_W \Lambda B_W + \mathcal{O}(\epsilon^2), \tag{3.3}$$

where Λ stands for the Poisson bracket operator:[62]

$$A_W \Lambda B_W = \{A_W, B_W\} = \nabla_P A_W \cdot \nabla_R B_W - \nabla_R A_W \cdot \nabla_P B_W.$$
(3.4)

Applying this rule to the first-order nonadiabatic coupling in the third term on the RHS of Eq. (2.16) we have[50]

$$(\epsilon C(R) \cdot \epsilon \nabla_R)_W = \epsilon C(R) \cdot i P - \frac{\epsilon^2}{2} \nabla_R \cdot C(R),$$
(3.5)

where all terms of higher order in ϵ vanish. Hence, the partial Wigner transform of the total Hamiltonian in adiabatic representation can be expressed by

$$H_W^{\mathrm{adi}}(R,P) = E(R) + \frac{1}{2}P^2 - i\epsilon C(R) \cdot P + \frac{\epsilon^2}{2}\nabla_R \cdot C(R)$$
$$- \frac{\epsilon^2}{2}T(R),$$
(3.6)

which again has to be understood as a matrix of functions in classical phase space.

C. Density operator

In this section the partial Wigner transforms of the density operator shall be derived. First, the diabatic density matrix shall be considered. Inserting Eq. (2.21) into Eq. (3.1) with $R' = R - \epsilon \Xi/2$ and $R'' = R + \epsilon \Xi/2$, it is straightforward to obtain the transform of the density. It can be written as a matrix of Wigner distribution functions in R and P with entries

$$\rho_{W,ij}^{\mathrm{dia}}(R,P,t) = \frac{1}{(2\pi)^D}\int_{R^D} X_{ij}^{\mathrm{dia}}\left(R - \frac{\epsilon}{2}\Xi, R + \frac{\epsilon}{2}\Xi, t\right)e^{iP\cdot\Xi}d\Xi$$
$$\equiv X_{W,ij}^{\mathrm{dia}}(R,P,t),$$
(3.7)

where each of the matrix elements simply equals the Wigner transform of the density of the heavy-particles only. Using the adiabatic representation (2.26) this expression for the partial Wigner transform has to be replaced by

$$\rho_{W,ij}^{\mathrm{adi}}(R,P,t) = \frac{1}{(2\pi)^D}\int_{\mathbf{R}^D} X_{ij}^{\mathrm{adi}}\left(R - \frac{\epsilon}{2}\Xi, R + \frac{\epsilon}{2}\Xi, t\right)$$
$$\times e^{iP\cdot\Xi}d\Xi - \frac{\epsilon}{2(2\pi)^D}\int_{\mathbf{R}^D}\Xi \cdot [(CX^{\mathrm{adi}})_{ij}$$
$$+ (X^{\mathrm{adi}}C)_{ij}]e^{iP\cdot\Xi}d\Xi + \mathcal{O}(\epsilon^2)$$
$$= X_{W,ij}^{\mathrm{adi}}(R,P,t) + \frac{i\epsilon}{2}$$
$$\times ([C(R),\nabla_P X_W^{\mathrm{adi}}(R,P,t)]_+)_{ij} + \mathcal{O}(\epsilon^2),$$
(3.8)

where $[C,\nabla_P X_W^{\mathrm{adi}}]_+ = \Sigma_{k=1}^D [C^k, \nabla_{P_k} X_W^{\mathrm{adi}}]_+$ stands for a generalized form of the anti-commutator $[A,B]_+ = AB + BA$ and where X_W^{adi} is defined in analogy to X_W^{dia} in Eq. (3.7) but for the adiabatic heavy-particle densities. As stated previously, the first-order correction term is due to the fact that the adiabatic basis for the light-particle Hamiltonian parametrically depends on the coordinates R of the heavy-particles.

D. Quantum-classical Liouville equation

In order to obtain a quantum-classical equation of motion for the system under consideration, we have to calculate a partial Wigner transform of the quantum Liouville equation (2.8). Replacing all expressions by the respective transforms and using again the first-order expression for the Wigner transform (3.3) of products of operators one readily obtains the QCLE

$$\partial_t \rho_W = -\frac{i}{\epsilon}[(H\rho)_W - (\rho H)_W]$$
$$= -\frac{i}{\epsilon}[H_W, \rho_W]_- - \frac{1}{2}(\{H_W, \rho_W\} - \{\rho_W, H_W\})$$
$$+ \mathcal{O}(\epsilon).$$
(3.9)

As will become more evident in the following section, the first term on the right-hand side of the above equation describes the purely quantum dynamics of the light-particles while the second and third terms contain both the dynamics of the heavy-particles and genuinely quantum-classical terms.

In order to apply this equation to a particular system we have to choose a certain representation for the transformed density ρ_W and the transformed Hamiltonian H_W. Using the diabatic representation introduced above, we have to insert Eqs. (3.2) and (3.7) into Eq. (3.9). Evaluating the commutator and the Poisson brackets we obtain the *diabatic QCLE*

$$\partial_t X_W^{\mathrm{dia}}(R,P,t) = -\frac{i}{\epsilon}[V(R), X_W^{\mathrm{dia}}(R,P,t)]_-$$
$$- P \cdot \nabla_R X_W^{\mathrm{dia}}(R,P,t)$$
$$+ \frac{1}{2}[\nabla_R V(R), \nabla_P X_W^{\mathrm{dia}}(R,P,t)]_+ + \mathcal{O}(\epsilon).$$
(3.10)

Similarly, by inserting Eqs. (3.6) and (3.8) into Eq. (3.9) the *adiabatic QCLE* is derived:

$$\partial_t X_W^{\mathrm{adi}}(R,P,t) = -\frac{i}{\epsilon}[E(R) - i\epsilon P \cdot C(R), X_W^{\mathrm{adi}}(R,P,t)]_-$$
$$+ \frac{1}{2}[E(R),[C(R),\nabla_P X_W^{\mathrm{adi}}(R,P,t)]_+]_-$$
$$- P \cdot \nabla_R X_W^{\mathrm{adi}}(R,P,t)$$
$$+ \frac{1}{2}[\nabla_R E(R), \nabla_P X_W^{\mathrm{adi}}(R,P,t)]_+ + \mathcal{O}(\epsilon).$$
(3.11)

E. Discussion

It is worthwhile to compare the present derivation of the quantum-classical Liouville equation with other approaches in the literature. Based on previous work on semiclassical propagators by Krause *et al.*,[63] Mukamel,[57] Martens and co-workers,[38,39,64] and Hartmann *et al.*[65] have used quantum-classical equations of motion which are very similar to the

ones obtained here. However, they used a truncated Wigner-Moyal series expansion for the transform of products [see Eq. (3.3)] in $\hbar$ and not in $\epsilon = \sqrt{m/M}$. Hence, their expressions reflect the traditional derivation of classical dynamics in the $\hbar \to 0$ limit.[66] The expansion in the smallness parameter ϵ was introduced in more recent work to rigorously establish a quantum-classical limit of the quantum Liouville equation.[47,50]

Furthermore, we would like to emphasize that in the present study the original quantum Liouville equation (2.3) describing the full quantum dynamics is first expressed in a (diabatic or adiabatic) representation and then (partially) Wigner transformed. This is in contrast to other recent studies where the density and Hamiltonian operator are first Wigner transformed and then expressed in a (diabatic or adiabatic) representation.[38,47–49,53–55,64] Although being formally equivalent, those studies give the evolution directly in terms of the heavy particle densities X_W^{adi}. Our approach, however, also allows for the construction of an equation of motion for the full adiabatic density ρ_W^{adi} by direct insertion of Eq. (3.6) into Eq. (3.9) without using Eq. (3.8). The resulting QCLE for ρ_W^{adi} is identical to Eq. (3.11) but does not contain the second commutator which is difficult to treat numerically because of the nonlocal operator ∇_P (see below). Nevertheless, it has been shown that the simplified propagation yields a $\mathcal{O}(\epsilon)$ approximation to the quantum-classical expectation values of physical quantities:[50]

$$\langle A \rangle_W = \int_{\mathbf{R}^D} \int_{\mathbf{R}^D} \text{tr}(X_W^{\text{adi}} A_W^{\text{adi}}) dR dP. \tag{3.12}$$

Furthermore, note that X_W^{adi} and ρ_W^{adi} coincide in spatial regions with vanishing kinetic coupling $C(R)$. This is of practical importance for simulations where both the initial and final states are far from the coupling regions. In these cases it is sufficient to propagate ρ_W^{adi} instead of X_W^{adi} if intermediate steps are not to be considered.

IV. NUMERICAL REALIZATION

A. Superoperator splitting

In the following we want to construct a numerical propagator for the solution of the adiabatic QCLE (3.11) neglecting all first- and higher-order terms in the smallness parameter ϵ. Using a simplified notation $X = X_W^{\text{adi}}$, the evolution of the adiabatic density can be expressed as

$$\partial_t X(R,P,t) = -\frac{i}{\epsilon} \hat{\mathcal{L}} X(R,P,t), \tag{4.1}$$

with the formal solution

$$X(R,P,t) = \exp\left(-\frac{it}{\epsilon} \hat{\mathcal{L}}\right) X(R,P,0). \tag{4.2}$$

In close analogy to the use of Trotter or Strang splitting schemes for the solution of the time-dependent Schrödinger equation,[67–69] a numerical solution of the adiabatic QCLE is realized by a Trotter splitting of the time evolution superoperator into three parts

$$\hat{\mathcal{L}} = \hat{\mathcal{L}}_1 + \hat{\mathcal{L}}_2 + \hat{\mathcal{L}}_3, \tag{4.3}$$

which allows for a discretization of the solution (4.2) using small time steps $\tau = \mathcal{O}(\epsilon)$,

$$X(R,P,t+\tau) = \exp\left(-\frac{i\tau}{\epsilon} \hat{\mathcal{L}}_1\right) \exp\left(-\frac{i\tau}{\epsilon} \hat{\mathcal{L}}_2\right)$$
$$\times \exp\left(-\frac{i\tau}{\epsilon} \hat{\mathcal{L}}_3\right) X(R,P,t) + \mathcal{O}(\epsilon^2), \tag{4.4}$$

where the individual superoperators are given by

$$-\frac{i}{\epsilon} \hat{\mathcal{L}}_1 X(R,P,t) = -\frac{i}{\epsilon} [E(R), X(R,P,t)]_-, \tag{4.5}$$

$$-\frac{i}{\epsilon} \hat{\mathcal{L}}_2 X(R,P,t) = [-P \cdot C(R), X(R,P,t)]_-$$
$$+ \frac{1}{2} [E(R), [C(R), \nabla_P X(R,P,t)]_+]_-, \tag{4.6}$$

$$-\frac{i}{\epsilon} \hat{\mathcal{L}}_3 X(R,P,t) = -P \cdot \nabla_R X(R,P,t)$$
$$+ \frac{1}{2} [\nabla_R E(R), \nabla_P X(R,P,t)]_+. \tag{4.7}$$

In the following we want to discuss the propagators associated with $\hat{\mathcal{L}}_1$, $\hat{\mathcal{L}}_2$, and $\hat{\mathcal{L}}_3$ individually. For the sake of simplicity consider a representation of the light-particle Hamiltonian that consists of two states only. Assuming the diabatic potential matrix V to be real and symmetric, we obtain the following eigenvalues:

$$E_{1,2}(R) = \frac{1}{2}[V_{11}(R) + V_{22}(R)]$$
$$\pm \frac{1}{2}\sqrt{[V_{11}(R) - V_{22}(R)]^2 + 4V_{12}^2(R)}. \tag{4.8}$$

The corresponding first-order kinetic coupling matrix is found to be real and antisymmetric with off-diagonal elements:

$$C_{12}(R) = -C_{21}(R) = \frac{[V_{11}(R) - V_{22}(R)]\nabla_R V_{12}(R) - V_{12}(R)\nabla_R[V_{11}(R) - V_{22}(R)]}{[V_{11}(R) - V_{22}(R)]^2 + 4V_{12}^2(R)}. \tag{4.9}$$

In the following we will replace the (real) densities and the (complex) coherences by a set of four real-valued phase-space functions. We introduce the sum and difference of the densities,

$$\sigma(t) = \tfrac{1}{2}[X_{11}(t) + X_{22}(t)], \tag{4.10}$$

$$\delta(t) = \tfrac{1}{2}[X_{11}(t) - X_{22}(t)], \tag{4.11}$$

along with the real and imaginary parts of the coherence:

$$r(t) = \mathrm{Re}[X_{12}(t)] = \tfrac{1}{2}[X_{12}(t) + X_{21}(t)], \tag{4.12}$$

$$j(t) = \mathrm{Im}[X_{12}(t)] = \frac{1}{2i}[X_{12}(t) - X_{21}(t)]. \tag{4.13}$$

Phase oscillations ($\mathcal{L}_1$). The time evolution connected with the first superoperator (4.5) affects only the coherences (off-diagonal elements of X) while leaving the densities (diagonal elements) unchanged. Hence, the time evolution can be re-written as

$$\partial_t \begin{pmatrix} r(t) \\ j(t) \end{pmatrix} = \begin{pmatrix} 0 & \omega \\ -\omega & 0 \end{pmatrix} \begin{pmatrix} r(t) \\ j(t) \end{pmatrix}, \tag{4.14}$$

the solution of which is a rotation in the plane of the complex numbers,

$$\begin{pmatrix} r(t+\tau) \\ j(t+\tau) \end{pmatrix} = \begin{pmatrix} \cos(\omega\tau) & \sin(\omega\tau) \\ -\sin(\omega\tau) & \cos(\omega\tau) \end{pmatrix} \begin{pmatrix} r(t) \\ j(t) \end{pmatrix}, \tag{4.15}$$

with Bohr frequency $\omega = (E_1 - E_2)/\epsilon$. Obviously, this evolution can be traced back to the quantum-mechanical commutator in Eq. (3.9) and is a purely quantum dynamical effect. While these phase oscillations can be neglected in the limit of very large energy gaps, they start to play an important role in the region of avoided crossings where the phase oscillates only slowly.

Exchange ($\mathcal{L}_2$). As a first step, let us consider the time evolution connected with the first term on the RHS of Eq. (4.6) only. Note that neglecting the second term corresponds to propagation of ρ instead of X [see Eq. (3.8)]. Then the time evolution reduces to

$$\partial_t \begin{pmatrix} \delta(t) \\ r(t) \end{pmatrix} = \begin{pmatrix} 0 & -2\zeta \\ +2\zeta & 0 \end{pmatrix} \begin{pmatrix} \delta(t) \\ r(t) \end{pmatrix}, \tag{4.16}$$

where we use the shorthand notation $\zeta = P \cdot C_{12}$. The solution of these coupled equations is given by

$$\begin{pmatrix} \delta(t+\tau) \\ r(t+\tau) \end{pmatrix} = \begin{pmatrix} \cos(2\zeta\tau) & -\sin(2\zeta\tau) \\ \sin(2\zeta\tau) & \cos(2\zeta\tau) \end{pmatrix} \begin{pmatrix} \delta(t) \\ r(t) \end{pmatrix}, \tag{4.17}$$

describing a rotation in the (δ, r) plane with an angular frequency of 2ζ. Note that the imaginary part $j(t)$ of the coherence is not affected. Hence, by changing $\delta(t)$, this propagator results in an exchange of density between the adiabatic states,

$$X_{11}(t+\tau) = \cos^2(\zeta\tau) X_{11}(t) + \sin^2(\zeta\tau) X_{22}(t)$$
$$- 2\sin(\zeta\tau)\cos(\zeta\tau) r(t), \tag{4.18}$$

$$X_{22}(t+\tau) = \sin^2(\zeta\tau) X_{11}(t) + \cos^2(\zeta\tau) X_{22}(t)$$
$$+ 2\sin(\zeta\tau)\cos(\zeta\tau) r(t), \tag{4.19}$$

where the first two terms on the RHS can be understood as Rabi-like oscillations of the populations and the third term stands for transitions induced by the coherence of the two states. At the same time, Eq. (4.16) describes a change of the (real part of the) coherence $r(t)$ which can be understood as a dephasing and rephasing of the corresponding wave functions in states 1 and 2.

If also the second term of Eq. (4.6) is taken into consideration, we encounter the nonlocal nature of the quantum-classical propagation through the momentum derivatives. The time evolution of $r(t)$ in Eq. (4.16) has to be replaced by

$$\partial_t r(R,P,t) = 2\zeta\,\delta(R,P,t)$$
$$+ [E_1(R) - E_2(R)]C_{12}(R) \cdot \nabla_P \sigma(R,P,t)$$
$$= \zeta\left(1 + \frac{S(R)}{2} \cdot \nabla_P\right) X_{11}(R,P,t)$$
$$- \zeta\left(1 - \frac{S(R)}{2} \cdot \nabla_P\right) X_{22}(R,P,t). \tag{4.20}$$

Assuming that the vector $S = (E_1 - E_2)C_{12}/\zeta$ is sufficiently small, as is the case in the vicinity of an avoided crossing, this can be approximated by

$$\partial_t r(R,P,t) \approx \zeta \exp\left(+\frac{S(R)}{2} \cdot \nabla_P\right) X_{11}(R,P,t)$$
$$- \zeta \exp\left(-\frac{S(R)}{2} \cdot \nabla_P\right) X_{22}(R,P,t)$$
$$= \zeta X_{11}\left(R, P + \frac{S(R)}{2}, t\right) - \zeta X_{22}\left(R, P - \frac{S(R)}{2}, t\right). \tag{4.21}$$

Hence, in the framework of the momentum jump approximation the transfer of population of the quantum system is associated with a change of the momentum of the classical system to compensate for the difference of the potential energies of the adiabatic states.[47]

Transport ($\mathcal{L}_3$). Finally, the propagator associated with the third part of the time evolution operator is investigated. Because E is diagonal, the commutator in Eq. (4.7) can be cast into purely classical Liouville equations describing a Hamiltonian flows for each entry of the density matrix,

$$\partial_t X_{ij}(R,P,t) = -\frac{i}{\epsilon}\left\{ E_{ij}(R) + \frac{1}{2}P^2, X_{ij}(R,P,t) \right\}, \tag{4.22}$$

where the effective potentials are given by $E_{ij} = (E_i + E_j)/2$: i.e., densities are transported along the corresponding adiabatic potential-energy surfaces while coherences are subject to an arithmetic mean potential.

Summary. A diagram of the Trotter splitting (4.4) of the adiabatic QCLE (3.11) is shown in Fig. 1. First, the phase oscillations of the coherence are illustrated by $\mathcal{L}_1$ mixing the real and imaginary parts $r(t)$ and $j(t)$ without changing the difference of populations, $\delta(t)$. Next the exchange operator
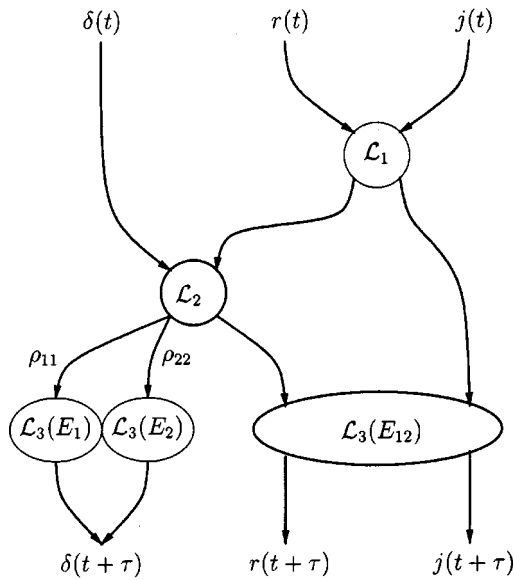
FIG. 1. Interplay of the three propagators: effect of $\mathcal{L}_1$ (phase oscillations), $\mathcal{L}_2$ (exchange), and $\mathcal{L}_3$ (transport) on the real-valued representation of the density matrix expressed as $\delta(t) = \frac{1}{2}[X_{11}(t) - X_{22}(t)]$, $r(t) = \text{Re}[X_{12}(t)]$, and $j(t) = \text{Im}[X_{12}(t)]$. While $\mathcal{L}_1$ and $\mathcal{L}_3$ can be described as rotations of the two quantities involved, the transport $\mathcal{L}_3$ acts differently on densities and coherences.

$\mathcal{L}_2$ mixes populations $\delta(t)$ and coherence $r(t)$. Finally, there is transport under the influence of $\mathcal{L}_3$ where each of the densities and coherence is transported along its own effective potential-energy surface.

A similar splitting scheme may also be applied to the diabatic QCLE (3.10). While eliminating the superoperator $\mathcal{L}_2$ due to the absence of kinetic coupling $C(R)$, there is exchange through the off-diagonal elements of the potential energy matrix $V(R)$ in $\mathcal{L}_1$. In contrast to the adiabatic description, this transfer of densities and coherence occurs on a fast time scale $\mathcal{O}(1/\epsilon)$ which makes the diabatic QCLE numerically much less favorable. In addition, the dynamics connected with $\mathcal{L}_3$ becomes more difficult through the advent of nonlocal operators connected with the potential coupling $V_{ij}(R)$.

B. Surface hopping trajectories

The simplest approach to a numerical solution of the adiabatic QCLE (3.11) leads to the well-known surface hopping trajectory (SHT) scheme which was originally derived empirically.[22–24] It is based on classical trajectories stochastically hopping between the adiabatic states of the quantum system. In order to demonstrate how this algorithm can be derived on the basis of the Trotter splitting of the adiabatic QCLE (4.4), we shortly summarize the concept of surface hopping in the following:

Representations. The densities are modeled using a set of (equally weighted) δ-like point particles in classical phase space:

$$X_{ii}(R,P,t) \approx \frac{1}{N_{ii}} \sum_{k=1}^{N_{ii}} \delta(R - R_{ii}^k(t)) \delta(P - P_{ii}^k(t)). \quad (4.23)$$

Assuming that the system is initially prepared in a single adiabatic state i, the ensemble of points $\{(R_{ii}, P_{ii})\}$ is obtained by Monte Carlo sampling from the initial Wigner distribution function $X_{ii}(R,P,t=t_0)$. If more than one adiabatic state is initially populated, the trajectories are distributed according to the respective densities. To allow for a coherent propagation, one has to associate a density matrix with each of the trajectories. The initial value of the density matrix is 1 in the corresponding diagonal element and zero elsewhere. Then time-dependent ensembles representing the multistate density at subsequent times are calculated by iterating the following three propagation steps for each member of the ensemble.

Phase oscillations $(\mathcal{L}_1)$. The purely quantum-mechanical time evolution associated with $\mathcal{L}_1$ is straightforward to realize by updating the phase of the coherence according to Eq. (4.15).

Exchange $(\mathcal{L}_2)$. The quantum-classical time evolution associated with $\mathcal{L}_2$ consists of two parts see [Eq. (4.6)]. The first one characterizing the exchange of densities and coherences is easily realized by updating the density matrix following Eq. (4.17). Upon linearization of the trigonometric functions [because $\tau = \mathcal{O}(\epsilon)$] in Eqs. (4.18) and (4.19), the change per time step of the diagonal elements reads[22]

$$P_{1 \leftarrow 2}(t) = X_{11}(t+\tau) - X_{11}(t) = -2\zeta\tau r(t), \quad (4.24)$$

$$P_{2 \leftarrow 1}(t) = X_{22}(t+\tau) - X_{22}(t) = 2\zeta\tau r(t), \quad (4.25)$$

which determines the probability for a sudden hop of a trajectory from one quantum state to the other one. In practice, a hop from state i to state j is realized whenever the probability $P_{j \leftarrow i}$ exceeds a random number $0 < \aleph < 1$. The second part of the propagator (4.6) associated with $\mathcal{L}_2$ can only be treated in the framework of the "momentum jump" approximation of Eq. (4.21) while a direct solution of Eq. (4.20) cannot be implemented within the framework of the traditional SHT approach. The momentum of the trajectories hopping between states is changed such as to ensure conservation of the sum of the potential and kinetic energies,

$$\tfrac{1}{2}P_{jj}^2 + E_j(R^k) = \tfrac{1}{2}P_{ii}^2 + E_i(R^k), \quad (4.26)$$

which implies the possibility of rejecting energetically forbidden transitions, where the kinetic energy is not sufficient to compensate a hop to an energetically higher state. Note that this is a reason often cited for the internal inconsistency of the trajectory-based method.[26,28]

Transport $(\mathcal{L}_3)$. The purely classical time evolution associated with $\mathcal{L}_3$ is realized by transporting all members of the ensemble along their respective potential-energy surfaces $E_i(R)$ according to Eq. (4.22). This can be achieved by any of the algorithms commonly used in classical molecular dynamics simulations,[70] e.g., the symplectic Verlet algorithm.

Discussion. The obvious shortcoming of the SHTs algorithm is that it does not correctly account for the transport of coherences. Instead it is assumed that a complete density matrix is propagated with each of the trajectories in the ensemble, thus enforcing the coherences to be transported along with the densities. In realistic quantum molecular dy-

namics, however, one generally observes the coherences to be transported into different regions of phase space as indicated by the different effective potentials in Eq. (4.22). This usually leads to a decay of coherence at the position of the densities. Hence, the traditional SHT algorithm typically overestimates the coherence at the position where, e.g., the RHS of Eqs. (4.24) and (4.25) has to be evaluated. Note that there exist suggestions to remedy the problem of "overcoherence" in the literature.[31,32]

C. Surface hopping Gaussian phase-space packets

In order to overcome the above-mentioned disadvantage of the traditional trajectory-based surface hopping algorithm one can follow two different approaches: One obvious possibility is to model the evolution of the coherences by sets of trajectories with complex-valued weights. For an N-state problem one has to propagate $N(N+1)/2$ phase-space functions instead of N functions in the traditional SHT approach described above.[22] While this does not present a major obstacle for simulations where the dynamics is determined by a few states only, a more serious problem arises. In order to evaluate equations such as Eqs. (4.16)–(4.21), we need information about the coherence to propagate the density at a certain point in phase space and vice versa. This type of information is *a priori* not available in the SHT approach where phase-space functions are sampled by δ-like particles in phase space. A way to circumvent this problem is the use of spawning or multithreading algorithms which generate new particles where needed. Despite the successful application of such algorithms for a number of prototypical problems in photophysics and photochemistry,[55] the principle limitation of this method lies in the rapidly growing number of particles with increasing time.

Representations. In the present work we rather suggest an alternative approach to propagate both densities and coherences: In order to achieve a dense sampling of the classical phase-space functions, one can represent them as a sum of traveling GPPs replacing the classical point particles in Eq. (4.23),

$$X_{ij}(R,P,t) \approx \sum_{k=1}^{N_{ij}} A_{ij}^{k}(t) g_{ij}^{k}(R,P,t), \qquad (4.27)$$

where the amplitudes $A_{ij}^{k}(t)$ of the Gaussians are real or complex for the densities ($i=j$) or for the coherences ($i \neq j$), respectively. Each of the Gaussian phase-space packets in the above equation is parametrized in the following way:

$$g_{ij}^{k}(R,P,t) = \exp\{-\alpha_{ij}^{k}(t)[R-R_{ij}^{k}(t)]^2 - \beta_{ij}^{k}(t)[P-P_{ij}^{k}(t)]^2$$
$$- \gamma_{ij}^{k}(t)[R-R_{ij}^{k}(t)][P-P_{ij}^{k}(t)]\}, \qquad (4.28)$$

where $R_{ij}^{k}(t), P_{ij}^{k}(t)$ give the position of the center of the packet in phase space, and $\alpha_{ij}^{k}(t), \beta_{ij}^{k}(t), \gamma_{ij}^{k}(t)$ specify the length and rotation of the axes of the elliptical contour of the packet. Note that the dense sampling by GPPs allows to evaluate phase-space functions at any given point (R,P) which is impossible for trajectory-based methods. For a mathematical proof of convergence of particle methods for Liouville-type equations see Ref. 71.

The initial set of GPPs is obtained from the initial Wigner distribution function $X_{ii}(R,P,t=t_0)$ by means of a novel algorithm for the optimal decomposition into GPPs at a given accuracy. For details the reader is referred to Ref. 72. Using the ansatz of Eqs. (4.27) and (4.28), a propagator of the adiabatic QCLE using the Trotter splitting technique (4.4) is constructed as follows:

Phase oscillations ($\mathcal{L}_1$). The purely quantal evolution (4.14) simply results in phase oscillations of the coherences which can be achieved by updating the (complex) amplitudes of the GPPs by multiplication with the highly oscillatory phase factors,

$$A_{ij}^{k}(t+\tau) = A_{ij}^{k}(t)\exp(-i\omega_{ij}\tau), \qquad (4.29)$$

with the Bohr frequency $\omega_{ij} = (E_i - E_j)/\epsilon$.

Exchange ($\mathcal{L}_2$). The quantum-classical exchange of densities and coherences is realized in the following way: In analogy to the trajectory-based surface hopping (SHT) explained in the previous section, we allow for a hopping of the GPPs representing the densities according to the same criterion (4.24) and (4.25) evaluated at the center of each of the GPPs. Note that there is no adjustment of the momentum of the hopping GPP because the second commutator in Eq. (3.11) can be treated beyond the momentum jump approximation (see below).

Following the hopping process, the densities and coherences have to be updated such as to fulfill the rotation given in Eq. (4.17) as close as possible. The simplest way to achieve this is by readjusting the amplitudes only, while leaving the other parameters of the GPPs unchanged. Consider, e.g., the change of density X_{11} in the first adiabatic state. Evaluation of the LHS of Eq. (4.18) at given points (R^l, P^l) in phase space leads to the following expression for the density after propagation for a time step τ:

$$X_{11}(R^l,P^l,t+\tau) = \sum_{k=1}^{N_{11}} A_{11}^{k}(t+\tau) g_{11}^{k}(R^l,P^l,t+\tau),$$
$$l = 1,\ldots,N_{11}. \qquad (4.30)$$

This allows us to rewrite Eq. (4.18) as a set of coupled linear equations,

$$G \cdot a = y, \qquad (4.31)$$

where a is the vector formed by the unknown "new" amplitudes $a_k = A_{11}^{k}(t+\tau)$, and y is the vector formed by the RHS of Eq. (4.18) evaluated at the points (R^l, P^l) using representation (4.27) in terms of known "old" GPPs:

$$y_l = \cos^2(\zeta\tau) \sum_{k=1}^{N_{11}} A_{11}^{k}(t) g_{11}^{k}(R^l,P^l,t)$$

$$+ \sin^2(\zeta\tau) \sum_{k=1}^{N_{22}} A_{22}^{k}(t) g_{22}^{k}(R^l,P^l,t)$$

$$- 2\sin(\zeta\tau)\cos(\zeta\tau) \sum_{k=1}^{N_{12}} \mathrm{Re}[A_{12}^{k}(t)] g_{12}^{k}(R^l,P^l,t).$$

$$(4.32)$$

Finally, the symbol G in Eq. (4.31) stands for the square matrix with elements

$$G_{lk} = g_{11}^k(R^l, P^l, t+\tau) = \exp\{-\alpha_{11}^k(t+\tau)[R^l - R_{11}^k(t+\tau)]^2$$
$$-\beta_{11}^k(t+\tau)[P^l - P_{11}^k(t+\tau)]^2$$
$$-\gamma_{11}^k(t+\tau)[R^l - R_{11}^k(t+\tau)][P^l - P_{11}^k(t+\tau)]\}, \quad (4.33)$$

where the quantities $R_{11}^k, P_{11}^k, \alpha_{11}^k, \beta_{11}^k, \gamma_{11}^k$ have already been propagated for a time step τ. A natural choice for the points (R^l, P^l) are the "new" centers $[R_{11}^k(t+\tau), P_{11}^k(t+\tau)]$ of the GPPs themselves, thus rendering the matrix elements to be identical to the overlap of the GPPs. Note that in realistic simulations the numerical solution of Eq. (4.31) is greatly facilitated by the fact that the matrix G is very sparse because the overlap practically vanishes for GPPs that are far from each other in phase space. Note that there is a variety of special algorithms designed for the efficient use of sparse systems.[73] The amplitudes of the GPPs representing the density of the second state, X_{22}, are obtained by evaluating Eq. (4.19) in the same way. Analogously, the update (4.20) of the complex amplitudes of the GPPs representing the coherence can be treated beyond the momentum jump approximation (4.21) by analytically evaluating the action of the nonlocal operators (∇_P) on the GPPs.

In summary, the solution of the above system of equations (4.31) yields the "new" amplitudes a in terms of the "old" amplitudes contained in y. It remains to be seen whether it may be useful to update the widths and centers of the GPPs, too. However, this would lead to a system of nonlinear equations. Instead, it may be advisable to circumvent this difficulty and to compensate the reduced flexibility of the individual GPPs by employing a larger number of them.

Transport ($\mathcal{L}_3$). The classical transport (4.22) of the densities and coherences along their respective effective potential-energy surfaces is realized in the framework of the locally quadratic approximation. Assuming that the GPPs are sufficiently narrow in position space, the potential-energy function is approximately locally quadratic over the spatial width of a packet,

$$E_{ij}(R) \approx E_{ij}(R_{ij}^k(t)) + \nabla_R E_{ij}(R_{ij}^k(t)) \cdot [R - R_{ij}^k(t)]$$
$$+ \tfrac{1}{2}\Delta_R E_{ij}(R_{ij}^k(t))[R - R_{ij}^k(t)]^2. \quad (4.34)$$

Inserting this ansatz together with the GPP representation (4.27) and (4.28) into the classical Liouville equation (4.22) leads to first-order equations of motion for the parameters of the GPPs (Ref. 56),

$$\partial_t R_{ij}^k(t) = P_{ij}^k(t),$$
$$\partial_t P_{ij}^k(t) = -\nabla_R E_{ij}(R_{ij}^k(t)),$$
$$\partial_t \alpha_{ij}^k(t) = \gamma_{ij}^k(t)\Delta_R E_{ij}(R_{ij}^k(t)),$$
$$\partial_t \beta_{ij}^k(t) = -\gamma_{ij}^k(t),$$
$$\partial_t \gamma_{ij}^k(t) = -2\alpha_{ij}^k(t) + 2\beta_{ij}^k(t)\Delta_R E_{ij}(R_{ij}^k(t)). \quad (4.35)$$

In analogy to earlier approaches to solve the time-dependent Schrödinger equation for the motion of Gaussian wave packets, the center of the packet follows Hamilton's classical equation of motion.[58] These equations are solved routinely in classical molecular dynamics simulations using, e.g., the leapfrog algorithm.[70] The width and shape of the GPPs are determined by the curvature of the potential-energy function. A modified leapfrog algorithm for an efficient solution of the above set of equations for GPP evolution which conserves both norm and energy has recently been developed.[72] Note that it is useful to monitor the GPP widths during propagation in order to check the validity of the locally quadratic representation of the potential-energy surface (4.34). Should the widths increase beyond a certain threshold given by a typical length scale of the potential-energy function, the simulation is suspended and the phase-space functions are refit by a new set of GPPs. A discussion of advanced algorithms for classical GPP dynamics which are adaptive both with respect to spatial and temporal discretization can be found in Ref. 74.

In multidimensional simulations the Laplacian in Eqs. (4.34) and (4.35) will have to be replaced by the Hessian matrix. While this information is available, e.g., from electron structure calculations for small to medium molecules, the calculation of the Hessian may represent a computational bottleneck for large molecules. In that case the "thawed" GPPs as defined in Eq. (4.28) will have to be replaced by "frozen" packets:[75] i.e., the shape matrices α, β, γ are assumed to be constant where the reduced flexibility will have to be compensated by using a larger number of GPPs.

Discussion. The principle of a SHG-based approach to the solution of the adiabatic QCLE by means of an ensemble of surface hopping GPPs should be clear from the previous three paragraphs. However, the initial conditions deserve some attention. First of all, let us discuss the representation of the densities. On the one hand, the GPPs have to be wide enough to guarantee a dense sampling of phase space. On the other hand, they have to be sufficiently narrow in position space in order to be subject to a locally quadratic potential energy function [see the approximation in Eq. (4.34)]. Similarly, the GPP widths have to be small compared with the spatial extension of the kinetic coupling $C(T)$. An algorithm for optimal decomposition of an initial density with a prespecified global error is described in Ref. 72.

Another issue is the initial representation of the coherences. Even when the initial coherences vanishes, i.e., if the system is initially prepared in a single adiabatic state, we need a set of GPPs with zero amplitudes to model the coherences. In the course of the propagation, their real part will acquire an amplitude due to the operation of $\mathcal{L}_2$ [see Eq. (4.16)], which shall be rotated in the complex number plane by virtue of $\mathcal{L}_1$ and transported by the action of $\mathcal{L}_3$ (see also Fig. 1). The use of grid methods as suggested in Ref. 39 clearly becomes prohibitive for multidimensional systems. Instead, we proceed as follows to generate the initial positions of the GPPs modeling the coherences: First, a trajectory-based surface hopping simulation is carried out. At each instance of time we are collecting those trajectories where coherence information is essential, i.e., where the hopping probability is large, and collect the respective triples (R_h, P_h, t_h). Should this set become exceedingly large, we
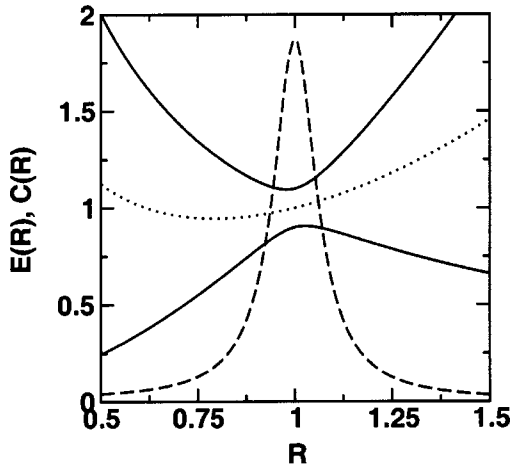
FIG. 2. Single-crossing example: adiabatic potential energy curves, $E_1(R)$ and $E_2(R)$, governing the transport of densities (solid line), mean-arithmetical surface, $E_{12}(R)$, for the transport of coherence (dotted line), and nonadiabatic coupling $C_{12}(R)/4$ (dashed line).

FIG. 3. Single-crossing example: population of upper adiabatic state versus time: numerically exact, fully quantum-mechanical simulation ("QM"), surface hopping trajectories ("SHT"), and surface hopping Gaussian phase-space packets ("SHG"). Note that for both the SHT- and SHG-based simulations 100 particles have been used.

introduce a Monte Carlo sampling from this set in order to obtain a smaller one. In a second step, each of these points in phase space is propagated back from t_h to initial time t_0. This supplies us with initial values for the centers $R_{ij}(t_0), P_{ij}(t_0)$. The corresponding width parameters are chosen such that a dense sampling of the coherences in phase space is guaranteed. Once we have completed the initial conditions, a forward simulation is performed, treating densities and coherences on the same footing, i.e., as a set of GPPs, as described in the three previous paragraphs. Again it is noted that the propagation of the densities and coherences might be performed adaptively through the techniques suggested in Ref. 74, i.e., GPPs can be generated or deleted as needed.

V. AVOIDED CROSSING EXAMPLES

A. Single crossing

In order to demonstrate the difference in the quality of approximation of a time evolving density matrix by the different surface hopping methods, we choose a single crossing characterized by the diabatic potential energy matrix,[50]

$$V_{11}(R) = AR^2, \quad V_{22}(R) = B/R, \quad V_{12}(R) = C, \quad (5.1)$$

with $A = B = 1$ and $C = 0.1$. The corresponding adiabatic potential-energy curves $E_1(R), E_2(R)$, exhibiting an avoided crossing, effective potential $E_{12}(R)$, and first-order nonadiabatic coupling C_{12}, are shown in Fig. 2. Initially, the system is assumed to be in a pure state, in this case the upper adiabatic state. It is characterized by a Gaussian wave packet in the heavy-particle degree of freedom,

$$\chi_1(R, t=0) \propto \exp\left(iP_0 R - \frac{1}{a^2}(R - R_0)^2 \right), \quad (5.2)$$

with $R_0 = 0.4$ which is located in the strongly repulsive regime of the upper adiabatic state, with initial momentum $P_0 = 100$ and with a width parameter of $a = 0.1$. The smallness parameter $\epsilon = \sqrt{m/M} = 0.01$ was chosen to resemble the mass ratio of electrons and nuclei typically encountered in molecular dynamics.
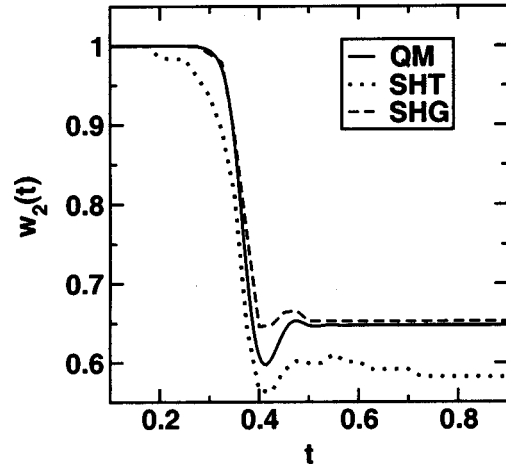
First of all, the numerically exact quantum evolution is generated as a reference for the quantum-classical propagation schemes. It is obtained in the Schrödinger picture using a grid representation in position space allowing for the efficient use of fast Fourier transforms (FFTs) for the evaluation of the kinetic energy operator.[76] The time discretization is accomplished by a second-order Strang splitting of the kinetic and potential parts of the Hamiltonian.[67–69] The resulting population dynamics can be seen in Fig. 3. Upon passing the region of the avoided crossing, the population of the upper state, $w_2(t) = \int dR |\chi_2(R,t)|^2$, decreases to 64%. Note the weak Stueckelberg oscillations that occur while the wave packet is still in the region of the crossing.

For the quantum-classical propagations the initial wave packet has to be transformed into phase space. The corresponding Wigner transform yields

$$X_{11}(R, P, t=0) \propto \exp\left(-\frac{a^2}{2}(P - P_0)^2 - \frac{2}{a^2}(R - R_0)^2 \right). \quad (5.3)$$

For the trajectory-based SHT method described in Sec. IV B, phase-space points are sampled from this distribution. For the novel GPP-based SHG method described in Sec. IV C, this distribution is decomposed into a number of narrow GPPs as described in Ref. 72 in more detail. Note that this decomposition works also for the more general case of Wigner distributions which are not positive everywhere. We compare the population of the upper state, $w_2(t) = \int dR \int dP \chi_{22}(R, P, t)$, obtained for 100 trajectories and GPPs, respectively, in Fig. 3. Using the same sequence of pseudorandom numbers for the stochastic treatment of the hopping process (4.24) and (4.25), the SHG method yields much better agreement with the fully quantal results than the SHT method. In principle, the results for the latter can be converged towards the numerically exact quantum-mechanical result by increasing the number of particles to a few thousand. This is because the packet passes the crossing
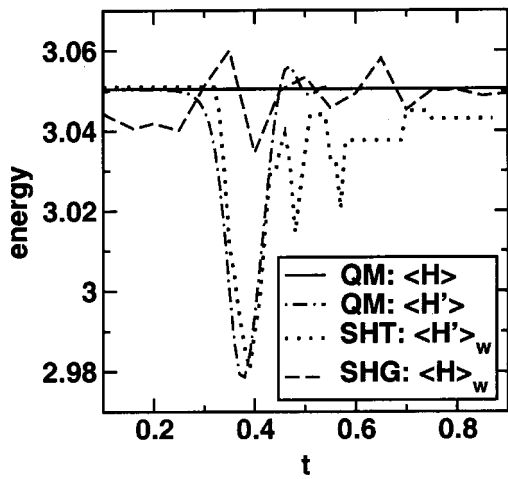
FIG. 4. Single-crossing example: expectation value of energy: numerically exact, fully quantum-mechanical simulation ("QM"), surface hopping trajectories ("SHT"), and surface hopping Gaussian phase-space packets ("SHG"). H stands for the total Hamiltonian: H' stands for the diagonal part (neglecting kinetic coupling).
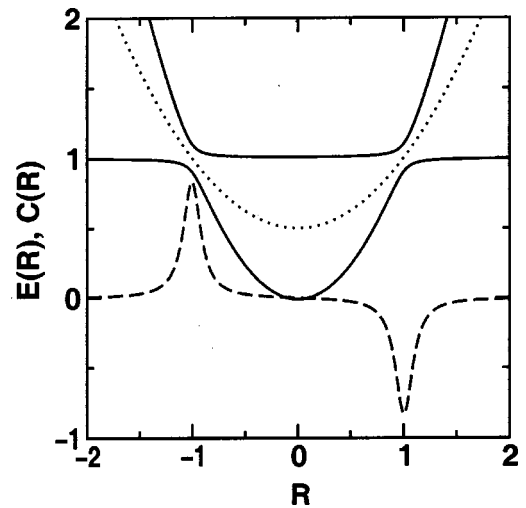

FIG. 5. Dual-crossing example: adiabatic potential energy curves, $E_1(R)$ and $E_2(R)$, governing the transport of densities (solid line), mean-arithmetical surface, $E_{12}(R)$, for the transport of coherence (dotted line), and nonadiabatic coupling $C_{12}(R)/6$ (dashed line).

region so fast that the transport of the coherence does not play an important role. Nevertheless, this result demonstrates the effect of better sampling of the densities in phase space by finite-width GPPs.

A similar picture emerges for the conservation of energy (see Fig. 4). The fully quantum-mechanical result obtained using the FFT-based split-operator scheme is numerically exact with the quantum-mechanical expectation value $\langle H \rangle$ for the (adiabatic) Hamiltonian of Eq. (2.16) being practically constant. For comparison, we also calculated the expectation value of the diagonal part $H'(R)=E(R)-\epsilon^2\Delta_R/2$ only, i.e., neglecting the kinetic coupling $C(R),T(R)$ in Eq. (2.16). The energy $\langle H' \rangle$ oscillates significantly as the wave packet passes the region of the avoided crossing. Note that these oscillations are in phase with the Stueckelberg oscillations of the population dynamics displayed in Fig. 3. A straightforward implementation of the SHT scheme without momentum adjustment shows that the course of $\langle H' \rangle$ can be qualitatively reproduced by the quantum-classical expectation value $\langle H' \rangle_W$ as defined in Eq. (3.12) where $H'_W(R,P)=E(R)+P^2/2$ is the diagonal part of Eq. (3.6). Note that the total energy $\langle H \rangle_W$ is not available for the traditional SHT method of Ref. 22. This behavior clearly indicates that the SHT algorithm without momentum adjustment (4.26) correctly reproduces the quantum result for the single-crossing example. On the contrary, applying the momentum adjustment would even deteriorate the result by enforcing an unphysical "energy conservation" for $\langle H' \rangle_W$ instead of $\langle H \rangle_W$. The result of the SHG-based simulation is also displayed in Fig. 4. Apart from statistical fluctuations the total energy $\langle H \rangle_W$ remains constant. Again, the results can be converged employing an increasing number of GPPs.

B. Dual crossing

The second model problem to be considered here consists of a pair of states exhibiting two avoided crossings. This case is much more demanding for any classically based theory due to the importance of possible interference effects

at the second crossing. Hence, a correct propagation of the densities and/or coherence in the region between the two crossings is of great importance. The diabatic interactions for our test model are

$$V_{11}(R)=AR^2, \quad V_{22}(R)=B, \quad V_{12}(R)=C, \qquad (5.4)$$

with the parameters chosen $A=B=1$ and $C=0.1$ (see Fig. 5). Note that for this example the gradient of the mean-arithmetic potential-energy surface $E_{12}(R)=[E_1(R)+E_2(R)]/2$ governing the transport of the coherence is significantly different from each of the adiabatic gradients for propagation of the densities. Initially, the system is assumed to be in the lower adiabatic state with a Gaussian-shaped wave function (5.2) or density (5.3) centered at $R_0=-4.0$ with initial momentum $P_0=20$, width $a_0=0.2991$, and
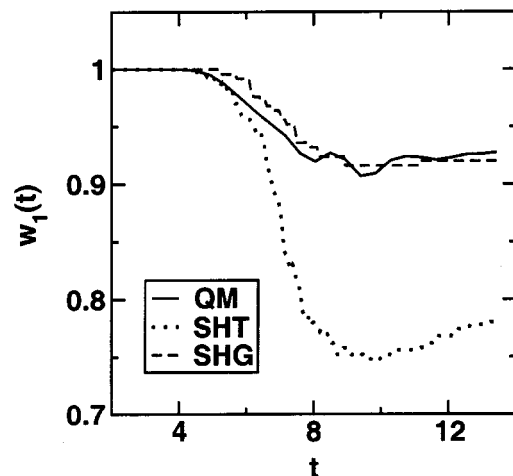

FIG. 6. Dual-crossing example: population of lower adiabatic state versus time for initial momentum $P_0=20$: numerically exact, fully quantum-mechanical simulation ("QM"), surface hopping trajectories ("SHT"), and surface hopping Gaussian phase-space packets ("SHG"). Note that for both the SHT- and SHG-based simulations 500 particles have been used.
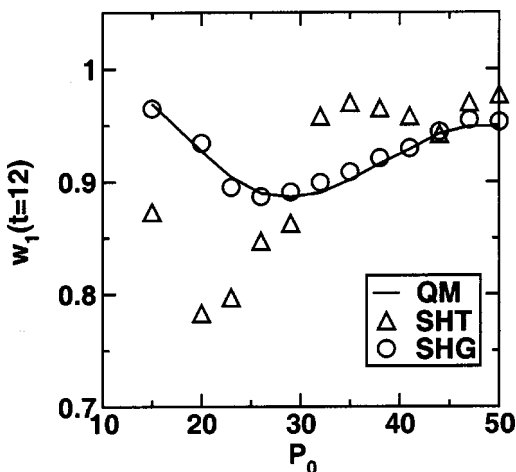
FIG. 7. Dual-crossing example: population of lower adiabatic state versus initial momentum of the wave packet for the final time $t = 12$: numerically exact, fully quantum-mechanical simulation ("QM"), surface hopping trajectories ("SHT"), and surface hopping Gaussian phase-space packets ("SHG").

smallness parameter $\epsilon = \sqrt{m/M} = \sqrt{1/2000}$. We used 500 trajectories or 500 GPPs to represent the densities and the same number to represent the coherence.

Our results are displayed in Fig. 6. The numerically exact quantum propagation displays the following behavior: Upon passing the first crossing at $R = -1$, about 10% of the population is transferred to the upper adiabatic state. Subsequently, the two parts of the wave packet arrive at the second crossing where the interference is such that the population is roughly unchanged: i.e., constructive and destructive effects are balancing each other. The population dynamics is reproduced correctly by the trajectory-based SHT procedure only for the time span of the passing of the first crossing ($t \leqslant 6$). At later times the overcoherent nature of this algorithm leads to a largely overestimated population transfer at the second crossing. This failure is remedied by the Gaussian-based SHG algorithm, yielding very good agreement with the fully quantum-mechanical simulation. This is a direct consequence of the correct modeling of the individual transport of densities and coherence. The failure of the trajectory-based method does not occur for the dual crossing example of Ref. 22 also investigated in Refs. 24, 54, and 59 where the potentials are constructed such that the adiabatic potential-energy surfaces $E_1(R)$ and $E_2(R)$ as well as $E_{12}(R)$ are approximately parallel. Note that the failure of the SHT approximation is also observed for different initial conditions. The dependence of the final time population of the lower adiabatic state on the initial momentum of the wave packet, P_0, is displayed in Fig. 7. Incidental agreement of SHT results with the quantum-mechanical results occurs only for specific values of P_0 while the SHG simulation correctly reproduces full quantum dynamics over the whole range of P_0.

VI. CONCLUSIONS

In the present work, a mixed quantum-classical model for the dynamics of large molecular systems has been worked out allowing for a quantum treatment of the most important degrees of freedom. More specifically, the quantum-classical Liouville equation has been derived as a first-order approximation to the partial Wigner transform of the quantum Liouville equation in the smallness parameter $\epsilon = \sqrt{m/M}$ characterizing the deviation from adiabatic behavior. Algorithms for the numerical treatment of the QCLE can be derived from a Trotter splitting of the time evolution superoperator and a stochastically based representation of densities and coherences. In particular it has been shown how the surface hopping trajectory procedure[22] can be derived from the QCLE essentially relying on two additional assumptions: namely, the momentum jump approximation and the transport of coherence along with the densities. The limitations of this approach can be overcome in the SHG approach using sets of surface hopping Gaussian phase-space packets to represent densities and coherences in phase space. The possibility to evaluate the action of nonlocal operators in phase space, too, allows us to perform simulations beyond the momentum jump approximation. The additional numerical effort for adjusting the amplitudes of the GPPs at every time step has to be compared with the main advantage over the multiple-threading algorithms which are limited by the steep rise of the number of particles with propagation time.[55] In contrast, the scheme proposed here requires only a modest number of GPPs because of the better sampling of phase space by a finite-width particle method.[71] These considerations make the novel algorithm especially promising in "on the fly" combination of molecular dynamics with *ab initio* calculations of the electronic structure where each trajectory is numerically very expensive.

Another field where the Gaussian-based SHG algorithm is potentially very useful is the dynamics of molecules interacting with (pulsed) light. Previous attempts at applying the trajectory-based SHT approach to such situations have been hampered by difficulties with the treatment of the coherence, limiting the use of this method to the regime of long wavelengths.[77,78] In recent work this problem is overcome by a stochastic implementation using particle hopping between different Floquet states of the "dressed molecule."[79]

[1] *Dynamics of Molecules and Chemical Reactions*, edited by R. E. Wyatt and J. Z. H. Zhang (Dekker, New York, 1996).
[2] *Computational Molecular Dynamics: Challenges, Methods, Ideas. Proceedings of the 2nd International Symposium "Algorithms for Macromolecular Modelling,"* edited by P. Deuflhard, J. Hermans, B. Leimkuhler, A. Mark, B. Skeel, and S. Reich, Lecture Notes in Computational Science and Engineering No. 4 (Springer, Berlin, 1998).
[3] *Femtochemistry and Femtobiology: Ultrafast Reaction Dynamics at Atomic-Scale Resolution*, edited by V. Sundström (Imperial College Press, London, 1997).
[4] *Classical and Quantum Dynamics in Condensed Phase Simulations*, edited by B. J. Berne, G. Ciccotti, and D. F. Coker (World Scientific, Singapore, 1998).

[5] V. May and O. Kühn, *Charge and Energy Transfer Dynamics in Molecular Systems* (Wiley-VCH, Berlin, 2000).

[6] P. K. Agarwal, S. P. Webb, and S. Hammes-Schiffer, J. Am. Chem. Soc. **122**, 4803 (2000).

[7] S. P. Webb, P. K. Agarwal, and S. Hammes-Schiffer, J. Phys. Chem. B **104**, 8884 (2000).

[8] J. Michl and V. Bonačić-Koutecký, *Electronic Aspects of Organic Photochemistry* (Wiley, New York, 1990).

[9] W. Domcke and G. Stock, Adv. Chem. Phys. **100**, 1 (1997).

[10] H.-D. Meyer and W. H. Miller, J. Chem. Phys. **70**, 3214 (1979).

[11] R. B. Gerber, V. Buch, and M. A. Ratner, J. Chem. Phys. **77**, 3022 (1982).

[12] R. B. Gerber and M. A. Ratner, J. Phys. Chem. **92**, 3252 (1988).

[13] F. A. Bornemann, P. Nettesheim, and C. Schütte, J. Chem. Phys. **105**, 1074 (1996).

[14] F. A. Bornemann and C. Schütte, SIAM (Soc. Ind. Appl. Math.) J. Appl. Math. **59**, 1208 (1999).

[15] P. Nettesheim, F. A. Bornemann, B. Schmidt, and C. Schütte, Chem. Phys. Lett. **256**, 581 (1996).

[16] H. J. C. Berendsen and J. Mavri, J. Phys. Chem. **97**, 13464 (1993).

[17] T. Terashima, M. Shiga, and S. Okazaki, J. Chem. Phys. **114**, 5663 (2001).

[18] P. Bala, P. Grochowski, B. Lesyng, and J. A. McCammon, J. Phys. Chem. **100**, 2535 (1996).

[19] J. Mavri and J. Grdadolnik, J. Phys. Chem. A **105**, 2045 (2001).

[20] D. Zahn and J. Brickmann, Phys. Chem. Chem. Phys. **3**, 848 (2001).

[21] J. C. Tully and R. K. Preston, J. Chem. Phys. **55**, 562 (1971).

[22] J. C. Tully, J. Chem. Phys. **93**, 1061 (1990).

[23] J. C. Tully, in *Classical and Quantum Dynamics in Condensed Phase Simulations*, edited by B. J. Berne, G. Ciccotti, and D. F. Coker (World Scientific, Singapore, 1998), pp. 700–720.

[24] D. F. Coker, in *Computer Simulation in Chemical Physics*, edited by M. P. Allen and D. J. Tildesley (Kluwer, Dordrecht, 1993), pp. 315–377.

[25] B. J. Schwartz, E. R. Bittner, O. V. Prezhdo, and P. J. Rossky, J. Chem. Phys. **104**, 5942 (1996).

[26] U. Müller and G. Stock, J. Chem. Phys. **107**, 6230 (1997).

[27] J.-Y. Fang and S. Hammes-Schiffer, J. Chem. Phys. **110**, 11166 (1999).

[28] J.-Y. Fang and S. Hammes-Schiffer, J. Phys. Chem. A **103**, 9399 (1999).

[29] M. F. Herman, J. Chem. Phys. **110**, 4141 (1999).

[30] K. Drukker, J. Comput. Phys. **153**, 225 (1999).

[31] E. R. Bittner and P. J. Rossky, J. Chem. Phys. **103**, 8130 (1995).

[32] E. R. Bittner and P. J. Rossky, J. Chem. Phys. **107**, 8611 (1997).

[33] Y. L. Volobuev, M. D. Hack, M. S. Topaler, and D. G. Truhlar, J. Chem. Phys. **112**, 9716 (2000).

[34] M. D. Hack, A. M. Wensmann, D. G. Truhlar, M. Ben-Nun, and T. J. Martinez, J. Chem. Phys. **115**, 1172 (2001).

[35] M. D. Hack and D. G. Truhlar, J. Chem. Phys. **114**, 9305 (2001).

[36] W. Boucher and J. Traschen, Phys. Rev. D **37**, 3522 (1988).

[37] O. Prezhdo and V. V. Kisil, Phys. Rev. A **56**, 162 (1997).

[38] C. C. Martens and J.-Y. Fang, J. Chem. Phys. **106**, 4918 (1997).

[39] A. Donoso and C. C. Martens, J. Phys. Chem. A **102**, 4291 (1998).

[40] A. Donoso and C. C. Martens, J. Chem. Phys. **112**, 3980 (2000).

[41] E. P. Wigner, Phys. Rev. **40**, 749 (1932).

[42] J. E. Moyal, Proc. Cambridge Philos. Soc. **45**, 99 (1947).

[43] K. Imre, E. Özizmir, M. Rosenbaum, and P. F. Zweifel, J. Math. Phys. **8**, 1097 (1967).

[44] M. Hillery, R. F. O'Connell, M. O. Scully, and E. P. Wigner, Phys. Rep. **106**, 121 (1984).

[45] P. Gerard, P. A. Markowich, N. J. Mauser, and F. Poupaud, Commun. Pure Appl. Math. **50**, 323 (1997).

[46] W. P. Schleich, *Quantum Optics in Phase Space* (Wiley-VCH, Berlin, 2001).

[47] R. Kapral and G. Ciccotti, J. Chem. Phys. **110**, 8919 (1999).

[48] S. Nielsen, R. Kapral, and G. Ciccotti, J. Chem. Phys. **112**, 6543 (2000).

[49] S. Nielsen, R. Kapral, and G. Ciccotti, J. Stat. Phys. **101**, 225 (2000).

[50] C. Schütte, Konrad-Zuse-Center, Report No. SC-99-10, 1999, available through http://www.zib.de/bib

[51] R. Kapral, J. Phys. Chem. A **105**, 2885 (2001).

[52] S. Nielsen, R. Kapral, and G. Ciccotti, J. Chem. Phys. **115**, 5805 (2001).

[53] C.-C. Wan and J. Schofield, J. Chem. Phys. **112**, 4447 (2000).

[54] C.-C. Wan and J. Schofield, J. Chem. Phys. **113**, 7047 (2000).

[55] M. Santer, U. Manthe, and G. Stock, J. Chem. Phys. **114**, 2001 (2001).

[56] J. Ma, D. Hsu, and J. E. Straub, J. Chem. Phys. **99**, 4024 (1993).

[57] S. Mukamel, *Principles of Nonlinear Optical Spectroscopy* (Oxford University Press, New York, 1995).

[58] E. J. Heller, J. Chem. Phys. **62**, 1544 (1975).

[59] T. J. Martinez, M. Ben-Nun, and R. D. Levine, J. Phys. Chem. **100**, 7884 (1996).

[60] M. Ben-Nun, J. Quenneville, and T. J. Martinez, J. Phys. Chem. A **104**, 5161 (2000).

[61] M. Ben-Nun, F. Molnar, H. Lu, J. C. Phillips, T. J. Martnez, and K. Schulten, Faraday Discuss. **110**, 447 (1998).

[62] H. Goldstein, *Classical Mechanics* (Addison-Wesley, Reading, MA, 1950).

[63] J. L. Krause, R. M. Whitnell, K. R. Wilson, and Y. J. Yan, in *Femtosecond Chemistry*, edited by J. Manz and L. Wöste (VCH, Weinheim, 1995), Vol. 2, Chap. 26, pp. 743–779.

[64] Z. Li, J.-Y. Fang, and C. C. Martens, J. Chem. Phys. **104**, 6919 (1996).

[65] M. Hartmann, J. Pittner, V. Bonacic-Koutecky, A. Heidenreich, and J. Jortner, J. Chem. Phys. **108**, 3096 (1998).

[66] E. J. Heller, J. Chem. Phys. **65**, 1289 (1976).

[67] M. D. Feit, J. A. Fleck, Jr., and A. Steiger, J. Comput. Phys. **47**, 412 (1982).

[68] M. D. Feit and J. A. Fleck, Jr., J. Chem. Phys. **78**, 301 (1983).

[69] A. D. Bandrauk and H. Shen, Can. J. Chem. **70**, 555 (1992).

[70] M. P. Allen and D. J. Tildesley, *Computer Simulations of Liquids* (Clarendon, Oxford, 1987).

[71] A. Arnold and F. Nier, Math. Comput. **58**, 645 (1992).

[72] I. Horenko, B. Schmidt, and C. Schütte, J. Chem. Phys. **117**, 4643 (2002).

[73] W. H. Press, S. A. Teukolsky, W. T. Vetterling, and B. P. Flannery, *Numerical Recipes in Fortran* (Cambridge University Press, Cambridge, England, 1992).

[74] I. Horenko and M. Weiser, Konrad-Zuse-Center, Report No. SC-02-29, 2002, available through http://www.zib.de/bib

[75] E. J. Heller, J. Chem. Phys. **75**, 2923 (1981).

[76] R. Kosloff, Annu. Rev. Phys. Chem. **45**, 145 (1994).

[77] M. Thachuk, M. Y. Ivanov, and D. M. Wardlaw, J. Chem. Phys. **105**, 4094 (1996).

[78] M. Thachuk, M. Y. Ivanov, and D. M. Wardlaw, J. Chem. Phys. **109**, 5747 (1998).

[79] I. Horenko, B. Schmidt, and C. Schütte, J. Chem. Phys. **115**, 5733 (2001).